Settling of Particles in Liquids: Effects of Material Properties

K. J. Dong, R. Y. Yang, R. P. Zou, and A. B. Yu
Laboratory for Simulation and Modelling of Particulate Systems, School of Materials Science and Engineering, University of New South Wales, Sydney, NSW 2052, Australia

DOI 10.1002/aic.12682
Published online June 16, 2011 in Wiley Online Library (wileyonlinelibrary.com).

This article presents a numerical study on the settling of uniform spheres in liquids by means of the discrete element method. The effects of particle and liquid properties, such as particle size, Hamaker constant, liquid density, and viscosity, on the formation of packed beds or cakes were studied in terms of packing fraction, radial distribution function (RDF), and coordination number (CN). The results showed that the packing fraction of a cake increases with increasing particle size but decreases with increasing the Hamaker constant, liquid density, and viscosity. RDF and CN also change correspondingly: packings with lower packing fraction generally have RDFs with fewer peaks and smaller mean CNs. A good correlation between packing fraction and other structural properties was identified. The analysis of the particle-particle and liquid-particle interactions showed that the packing properties are mainly affected by the ratio of the interparticle cohesion to the effective gravity of particles. The previously proposed equation linking packing fraction with the interparticle forces has been extended to incorporate the impact-induced pressure force in a settling process. Based on the modified equation, the effects of key variables on the relationship between packing fraction and particle size were re-examined for general application. © 2011 American Institute of Chemical Engineers *AIChE J,* 58: 1409–1421, 2012
Keywords: particle packing, cake formation, interparticle forces, discrete element method

Introduction

Particle settling in liquids is important to numerous industrial applications, such as mineral, biochemical, pharmaceutical, and petroleum industries.[1] For example, solid-liquid separation is a major unit operation in mineral processes in which particles are separated from slurry due to their density or size difference and settle down on a retaining medium to form a packed bed (often called as ''cake''). The formation and growth of such a cake are affected by many variables, e.g., particle size and size distribution, liquid density and viscosity and hence have been subjected to studies for many years.[2–10] Several macroscopic models have been formulated based on the balance and continuity of liquid and solid phases.[3,4] These models are often based on certain empirical assumptions which are condition-dependent, thus limiting their generality in application.[2]

To understand the cake structure and its evolution during a settling process, in the past a few semidynamic numerical models have been developed to trace the cake formation at a particle scale, such as the sticking model,[5] discrete stochastic model,[6] and kinetic force-balance model.[7] As the inter-particle forces in these models are either ignored or treated with assumptions, the models are difficult to study the effects of the forces on the cake formation. On the other hand, models based on the discrete element method (DEM)[11,12] are fully dynamic, describing the motion of individual particles and explicitly considering the interactions between particles and

Correspondence concerning this article should be addressed to A. B. Yu at a.yu@unsw.edu.au.

Table 1. Equations Used to Calculate Forces in this Work

Force	Equation
Particle-particle forces[13,18–20]	$\mathbf{F}_{ij}^{n} = \left[\frac{2}{3}\frac{Y}{1-\tilde{\sigma}^2}\sqrt{\bar{R}}\xi_n^{3/2} - \gamma_n \frac{Y}{1-\tilde{\sigma}^2}\sqrt{\bar{R}}\sqrt{\xi_n}\left(\mathbf{v}_{ij}\cdot\hat{\mathbf{n}}_{ij}\right)\right]\hat{\mathbf{n}}_{ij}$
	$\mathbf{F}_{ij}^{s} = \mu_s\lvert\mathbf{F}_{ij}^{n}\rvert\,[1-(1-\min(\xi_s,\,\xi_{s,\max})/\xi_{s,\max})^{3/2}]\hat{\boldsymbol{\xi}}_s$
	$\mathbf{F}_{ij}^{vdw} = -\frac{A}{6}\cdot\frac{64R_i^3R_j^3(h+R_i+R_j)}{(h^2+2R_ih+2R_jh)^2(h^2+2R_ih+2R_jh+4R_iR_j)^2}\hat{\mathbf{n}}_{ij}$
	where: $\hat{\mathbf{n}}_{ij} = (\mathbf{R}_i-\mathbf{R}_j)/\lvert\mathbf{R}_i-\mathbf{R}_j\rvert$, $\bar{R} = R_iR_j/(R_i+R_j)$,
	$\xi_{s,max} = \mu_s[(2-\tilde{\sigma})/2(1-\tilde{\sigma})]\xi_n$
Liquid-particle forces[21,22]	$\mathbf{F}_{buoy} = m\mathbf{g}\rho_f/\rho_p$
	$\mathbf{F}_{lift} = \frac{\pi}{8}\rho_f R_i^3(1-\varepsilon_i)\left[\left(\frac{1}{2}\nabla\times\mathbf{u}_f-\boldsymbol{\omega}_i\right)\times(\mathbf{u}_f-\mathbf{u}_i)\right]$
	$\mathbf{F}_{drag} = 0.5c_{d0,i}\rho_f\pi R_i^2\varepsilon_i^2\lvert\mathbf{u}_f-\mathbf{u}_i\rvert(\mathbf{u}_f-\mathbf{u}_i)\varepsilon_i^{-\chi}$
	where: $C_{d0,i} = (0.63+4.8/\mathrm{Re}_{p,i}^{0.5})^2$, $\mathrm{Re}_{p,i} = 2\rho_f R_i\varepsilon_i\lvert\mathbf{u}_f-\mathbf{u}_i\rvert/\mu_f$,
	$\chi = 3.7-0.65\exp(-0.5(1.5-\log_{10}\mathrm{Re}_{p,i})^2)$

between particles and fluid. DEM has been proved to be an useful technique to study the packing and flow of particles,[13,14] which is very much similar to the particle settling in a fluid.

A few attempts have been made to apply the DEM approach to model settling processes,[8–10] but they are two-dimensional or mainly qualitative. We recently developed a three-dimensional DEM model to simulate the settling of uniform spheres in liquids[15] and in a dead-end filtration process.[16] The results showed that the decrease in packing fraction (=1-porosity) is mainly due to the enhanced effect of the cohesion between particles as a result of the reduced gravity in liquids (gravity minus buoyancy force). The studies also revealed that packing fraction is dependent on the properties of liquids and particles, and as a result, the so-called random loose packing may correspond to a wide range of packing fractions, which is different from the previous work.[17] However, how the micro-structures of cakes are changed with the varying of packing fraction is not analyzed in any details, which is important to the permeability of cakes and hence to the performance of the settling processes, such as the pressure drop in filtrations. Moreover, it appears that different settling conditions give different relationships between packing fraction and inter-particle forces, which should be further explored.

In this work, we extend our previous studies[15,16] to overcome these gaps. First, different treatments for simulation will be examined to fully verify the approach. Then, the forces and structural properties in a settling process are analyzed in details, so as to establish better mechanistic understanding on how cake structures change under different settling conditions. It will be demonstrated that the cake structures can always be determined by a single macroscopic parameter, i.e., packing fraction. Based on the simulated results, an equation is formulated to link packing fraction to various inter-particle forces. The effects of particle and liquid properties on particle packing are comprehensively studied to produce some information for general application.

Numerical Model

The DEM model in this work is similar to that in the study of the packing of fine particles in vacuum or air.[13] However, modifications have been made to take into account various interaction forces for cohesive particles and fluid environment. In a DEM simulation, each particle possesses translational and rotational motions which can be described by Newton's second law of motion, given by:

$$m_i\frac{d\mathbf{v}_i}{dt} = \sum_j\left(\mathbf{F}_{ij}^{n}+\mathbf{F}_{ij}^{s}+\mathbf{F}_{ij}^{vdw}\right)+\mathbf{F}_{buoy,i}+\mathbf{F}_{drag,i}+\mathbf{F}_{lift,i}+m_i\mathbf{g} \tag{1}$$

and

$$I_i\frac{d\boldsymbol{\omega}_i}{dt} = \sum_j\left(\mathbf{R}_{ij}\times\mathbf{F}_{ij}^{s}-\mu_r R_i\left|\mathbf{F}_{ij}^{n}\right|\hat{\boldsymbol{\omega}}_i\right) \tag{2}$$

where $\boldsymbol{v}_i$, $\boldsymbol{\omega}_i$, and I_i are, respectively, the translational and angular velocities, and the moment of inertia of particle i, $\mathbf{R}_i$ a vector running from the center of the particle to the contact point with its magnitude equal to particle radius R_i, μ_r the rolling friction coefficient and $\hat{\boldsymbol{\omega}}_i = \boldsymbol{\omega}_i/\lvert\boldsymbol{\omega}_i\rvert$. $\mathbf{F}_{ij}^{n}$ and $\mathbf{F}_{ij}^{s}$ are the normal and tangential contact forces respectively, and $\mathbf{F}_{ij}^{vdw}$ is the van der Waals force between two particles. Due to the surface roughness, in calculating the van der Waals force, a minimum separation $h_{\min}$ = 1nm is assumed, i.e., when the surface gap of two particles h is less than this value, the van der Waals force has a constant and maximal value, a treatment that has been used in our previous studies.[13–15] The buoyancy ($\mathbf{F}_{buoy}$), drag ($\mathbf{F}_{drag}$) and Magnus lift

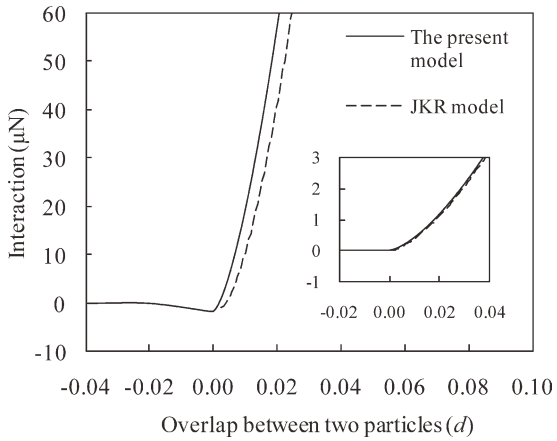

Figure 1. Interaction between two particles calculated by the present DMT-type model and the JKR model for 100 μm and (inset) 1000 μm particles when the Hamaker constant is 6.5×10^{-20} J.

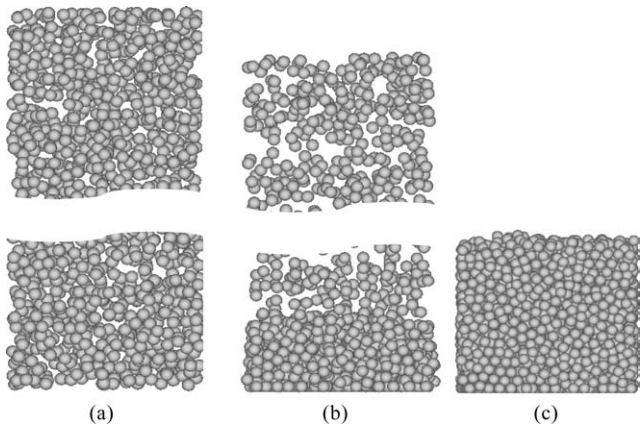

Figure 2. Snapshots showing the formation of a packing in settling process: (a) $t = 0$ s, (b) $t = 1.0$ s, (c) $t = 2.0$ s.

($\mathbf{F}_{lift}$) forces are included to describe the particle-fluid interactions. Table 1 lists the equations for the calculation of these forces.

There are two common models to calculate the adhesion between particles, namely, the DMT (Derjaguin, Muller, and Toporov) model[23] and JKR (Johnson, Kendall, and Roberts) model.[24] In the DMT model, the radius of the elastic deformation of a particle is calculated according to the Hertzian theory, while the adhesion force according to the Hamaker theory. On the other hand, the JKR model recognizes that both tensile and compressive interactions contribute to the total contact radius.[24] The present force model is in essence the same as the DMT model, where the mechanical contact and van der Waals forces are considered separately. It has been pointed out that the DMT theory is more suitable for small particles with high modulus and low surface energy, and the JKR theory is for large soft particles with high surface energy.[25] In Figure 1, we compare the total force between two contact particles calculated according to the two models for the current system. It suggests that the two models give comparable results, and the difference can only be observed for fine particles. In particular, our force model can give a smooth transition for two particles moving from non-contact to contact. Before the two particles are in contact, the interaction between them is attractive and increases with the decrease of their separation distance. The largest adhesion occurs when the two particles begin to contact, and with the increase of the overlap, the total interaction increases from negative representing an attractive force to positive representing a repulsive force. This transition is qualitatively in accordance with the experimental findings.[26]

Figure 2 shows snapshots at different times to illustrate the settling process. A simulation starts with the random generation of 3500 uniform spherical particles with no overlap in a rectangular box of a length equal to $15d$ (particle diameter). Periodic boundary conditions are applied to the horizontal directions to reduce the wall effect.[27] The particles are then allowed to settle down under the gravity and other forces mentioned above until the velocities of all particles are essentially zero to form a stable packing. Under the present conditions, the motion of liquid is very small compared with that of particles and is therefore ignored for simplicity. A cake grows vertically, but its structure is rather uniform as we did not observe any significant variation in (local) packing fraction in the vertical direction. It is worthwhile mentioning that although the structure is uniform, the forces between particles decrease with the packing height (from the top) because of the particle weight as will be shown later. This is because a tiny change of particle position, i.e., overlap between particles, although insignificant for the packing structure, is dramatically exemplified in the force structure because of the very large Young's modulus used to calculate the contact forces. The same reason applies to the packing of fine particles in air or vacuum.[28]

In this work, we mainly investigate the effects of four variables related to particle and liquid properties: particle size, liquid density and viscosity, and Hamaker constant. Table 2 lists the base value and the varying range of each variable considered. Unless otherwise stated, when studying the effect of a variable, only this variable is varied while others are set to their base values. For convenience, the bottom wall is assumed to have the same properties as particles but infinity large radius.

Results and Discussion

The numerical model is validated by comparing the simulated with the measured results, as reported in our previous

Table 2. Parameters Used in the Simulation

Parameter	Base Value	Varying Range
Particle size, d	250 μm	5–1000 μm
Particle density, ρ_p	2460 kg/m^3	–
Liquid density, ρ_f	1000 kg/m^3	500–2450 kg/m^3
Liquid viscosity, μ_f	0.001 kg/(ms)	0.0001–0.1 kg/(ms)
Hamaker constant, A	6.5×10^{-20}J	1.0×10^{-22} – 6.5×10^{-20} J
Young's modulus, Y	1.0×10^7 N/m^2	–
Damping coefficient, γ_n	2.0×10^{-5}	–
Sliding friction coefficient, μ_s	0.3	–
Rolling friction coefficient, μ_r	0.02	–

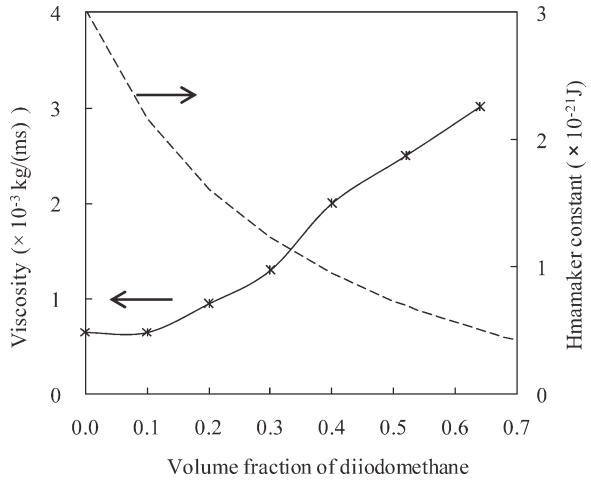

Figure 3. Variation of the measured liquid viscosity (solid line) and the estimated Hamaker constant (dashed line) with liquid composition.

work.[15] The physical experiments are conducted by settling mono-dispersed glass beads in a mixture of diiodomethane (density 3300 kg/m^3) and toluene (density 867 kg/m^3). The mixture density is controlled by adjusting the liquid composition, which is the volume weighted mean of the densities of the two liquids. Other liquid properties, such as viscosity and the Hamaker constant, vary more complicatedly. While the liquid viscosity is measured by a viscosity meter, the Hamaker constant of the glass beads in the liquid mixture is determined by two methods. One is assuming A is constant which gives the best fitted results at 1.0×10^{-21} J. And the other method is to set A as the weighted mean of the Hamaker constants for glass beads in pure toluene (3.0×10^{-21} J) and diiodomethane (1.0×10^{-22} J).[15] The estimated A as a function of liquid composition is shown in Figure 3. Figure 4 compares the simulated and measured packing fractions. It can be seen that both methods can give results comparable with the experimental data, which confirms the validity of our numerical model despite the uncertainty in determining the Hamaker constant. In the following, we will analyze the packing structure and forces based on the simulated results.

Packing structures

Figure 5 shows the effects of the variables considered on packing fraction. The results are actually re-plotted based on those reported elsewhere.[15] They are used here to establish some background for the present structural analysis. Figure 5a demonstrates that ρ decreases with increasing A, which is qualitatively consistent with the previous findings.[13] Quantitatively, the decrease is more significant in heavier liquids. This is because the increase in A means increasing the interparticle cohesion, which can suppress particle movements. For heavier liquids, the role of cohesion is further enhanced as the gravity force, the driving force to form a packing here, are neutralized by a larger buoyancy force, resulting in a looser packing structure. Similar trends are also observed from Figure 5b which shows that the packings of smaller particles have lower packing fractions. This is because the van der Waals force becomes more and more important in heavier liquids. Figures 5c, d show that increasing liquid density or viscosity decreases packing fractions. This is because an increased liquid density or viscosity will increase the resistant force to the motion of particles. Notably, if the interparticle cohesion is ignored ($A = 0$), the packing fraction is almost at a constant of 0.615. This highlights the critical role of the van der Waals force. The changes to other variables only enhance or weaken this role.

Particle rearrangement is necessary to generate a dense packing. Figure 6 shows the trajectory of a typical particle in a settling process. The particle firstly experiences the free settling period during which only its height (z) decreases. After the particle touches the underneath particles, it starts to rearrange its position, mainly in the x and y directions, until it reaches its stable position. Different packing conditions give different degrees of rearrangement and hence different packing fractions. Figure 7 shows that there is a relationship between packing fraction and particle rearrangement which is here measured by the average horizontal displacement, $S_d = \frac{1}{N}\sum_i^N \sqrt{(x_{i,t} - x_{i,0})^2 + (y_{i,t} - x_{i,0})^2}$, where N is the number of particles in a simulation, $x_{i,t}$ and $y_{i,t}$ are the two horizontal coordinates at the final state, while $x_{i,0}$ and $y_{i,0}$ are those at the initial state. Clearly, packing fraction can be related to the microdynamic behavior of individual particles.

Other structural properties also change in association with the change in packing fraction. Two common properties, radial distribution function (RDF) and coordination number (CN), are examined here. Figure 8 shows the variation of RDF with different variables. Figure 8a shows that the RDF of the packing of 1000 μm particles has a visible second peak, which is typical for the random packing of noncohesive particles. As particle size decreases and packing fraction decreases, the first peak in the RDF becomes narrower and the second peak becomes weaker gradually. These changes

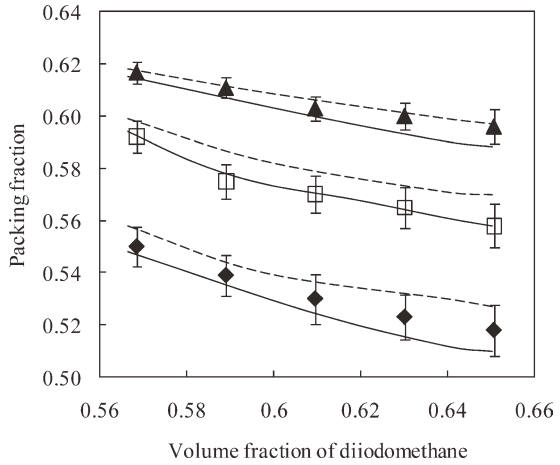

Figure 4. Packing fraction of different sized glass beads as a function of liquid composition.

Points are the measured results: ▲, $d = 500$ μm; □, $d = 250$ μm; ◆, $d = 110$ μm. Lines are the simulated results: solid lines are the results by setting $A = 1.0 \times 10^{-21}$ J, dashed line are the results by estimating A based on the liquid compositions (see Figure 3).

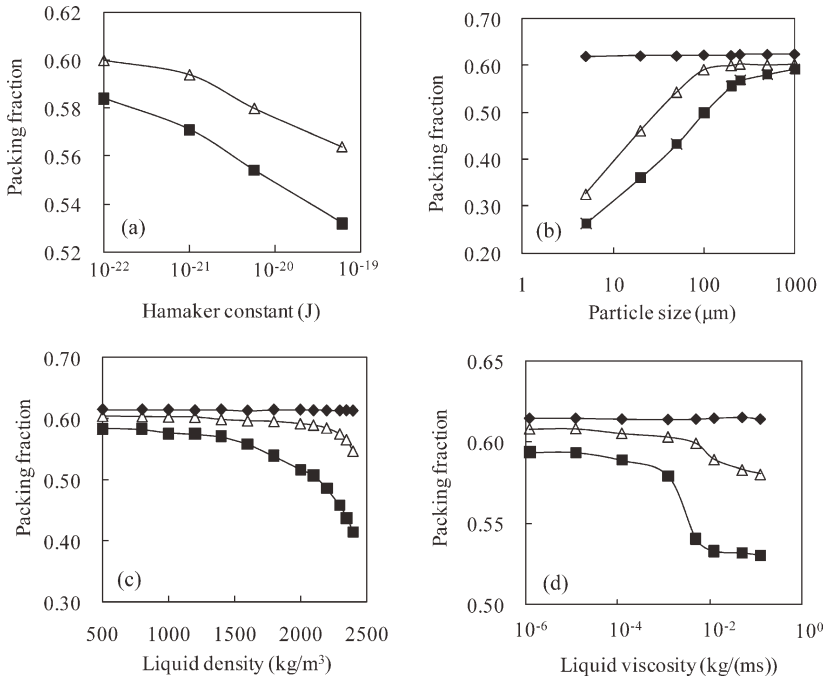

Figure 5. Packing fraction as a function of: (a) Hamaker constant with ρ_f = 2200 kg/m^3 (■) and ρ_f = 2400 kg/m^3 (Δ); (b) particle size with ρ_f = 0 kg/m^3 (■), ρ_f=1000 kg/m^3 (Δ) and A = 0 J (◆); (c) liquid density with d = 1000 μm (■), d = 250 μm (Δ) and A = 0 J (◆); (d) liquid viscosity with d = 1000 μm (■), d = 250 μm (Δ) and A = 0 J (◆).

Other parameters use the base values listed in Table 2.

are consistent with the packing of fine particles in air or vacuum[13,14] and suggest the ordered packing becomes more localized. The increase in liquid density or viscosity leads to similar changes in the RDF with decreasing packing fraction, as shown, respectively, in Figures 8b, c.

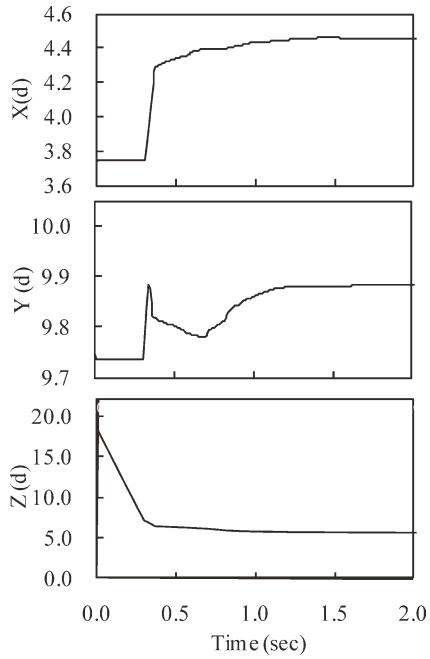

Figure 6. Coordinates of a selected particle as a function of time during the settling process.

Figure 9 shows the effects of these variables on the CN distribution. It should be noted that CN is dependent on the critical distance of separation less than which two particles are defined in contact. In this work, the distance is set to 0.005d (d is particle diameter), i.e., two particles are considered in contact if the distance between their centers is less than 1.005d. With the decrease of particle size, the most probable contact number decreases from 6 to 2 (Figure 9a). The decrease also occurs with increasing liquid density (Figure 9b) and liquid viscosity (Figure 9c),

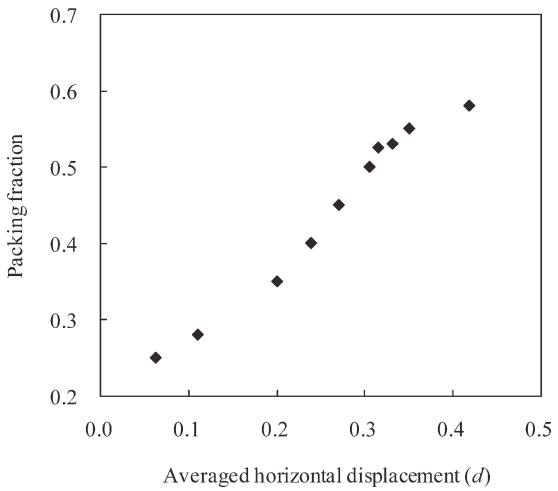

Figure 7. Packing fraction as a function of averaged horizontal movements of particles during the settling process.

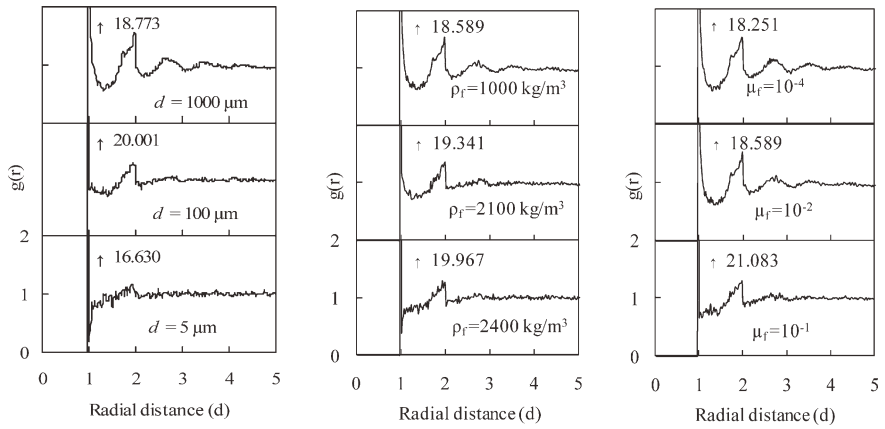

(a) (b) (c)

Figure 8. Variation of RDF with: (a), particle size; (b), liquid density; and (c), liquid viscosity.

indicating that the change of local packing structure is similar under these conditions. Indeed, as shown in Figure 10, there is a general correlation between the mean CN and packing fraction. This correlation can be described by the following equation[13]:

$$\overline{N} = N_0 \frac{1 + a\rho^4}{1 + b\rho^4} \tag{3}$$

where $\overline{N}$ is the mean CN, and parameters N_0, a, and b are, respectively, 2.02, 87.38, and 25.81.

It can be seen that both RDF and CN show similar variations when packing fraction decreases with the decrease of particle size, or the increases of liquid density and/or liquid viscosity. It was reported that there is a one-to-one relationship between packing fraction and the microstructural properties in the packings of coarse and fine particles in air.[14] Such relationship is also applicable to the packings formed in liquids. We plot in Figures 11 and 12, respectively, the RDF and CN distributions of the packings with similar packing fractions, with detailed conditions given in Table 3. Both figures demonstrate that the microstructures of the packings are similar when their packing fractions are close, despite that they are formed under different conditions. The results suggest that various properties affect the packings by a common mechanism, which should be related to the forces controlling the packing process, as packing is essentially a dynamics process governed by these forces.

Force analysis

The effects of particle and liquid properties can be further understood in terms of the forces controlling the settling process. The force information can be readily obtained from the simulations. Figure 13 shows the temporal variations of the forces for a single particle and all the particles on average under given settling conditions. They both show a similar trend which can be divided into three periods. The first period corresponds to a free settling process where a particle has a constant terminal velocity due to the balance among the gravity, buoyancy, and liquid drag forces. As the interactions with other particles are limited, the van der Waals force is negligible while the drag force has a maximum value. In the second period, the particle touches the already formed packing underneath and re-arranges itself to obtain its mechanically stable position. While the van der Waals force reaches the maximum value as the particle is in contact with others, the drag force decreases sharply with the decreasing velocity. In the third period, the particle has a very small oscillation in position and the drag force diminishes gradually. It is observed that the lift force is several orders of magnitude smaller than other forces so its effect can be ignored.

Figure 14 shows how the forces are affected by the key variables. It can be seen that decreasing the Hamaker constant and hence the van der Waals force (Figure 14a) leads to an increased re-arrangement time, as particles are less likely to stick to others. On the other hand, the increase in liquid density (Figure 14b) or viscosity (Figure 14c) increases the hindrance to the movements of particles when they collide and interact with others, hence reducing the re-arrangement time. They also increase the drag force and the lift force so that particles take a longer time to settle down.

The drag and lift forces are dependent on particle velocity and both will be zero once a packing reaches its final stage. The remaining forces are the contact force, van der Waals force, and buoyancy force, in addition to the gravity. The contact force is the most important and has been studied extensively.[28,29] Here, we study the spatial and statistical distributions of the contact force in cakes formed under different conditions. Figure 15 shows the spatial distribution for the normal contact forces of different packings. In the dense packing (Figure 15a), the large force chains (darker and thicker branches) exist at the bottom and propagate upwards. As the gravity force is dominant, particles need relatively larger contact forces to support particles above them. However, as a cake becomes looser due to the changes in particle size, liquid density, or viscosity, as shown in Figure 15b–d, the large force chains are less obvious at the bottom, indicating that the van der Waals force plays a more and more important role in balancing the gravity.

Figure 16 shows the statistical distributions of the contact forces for packings with similar packing densities that are

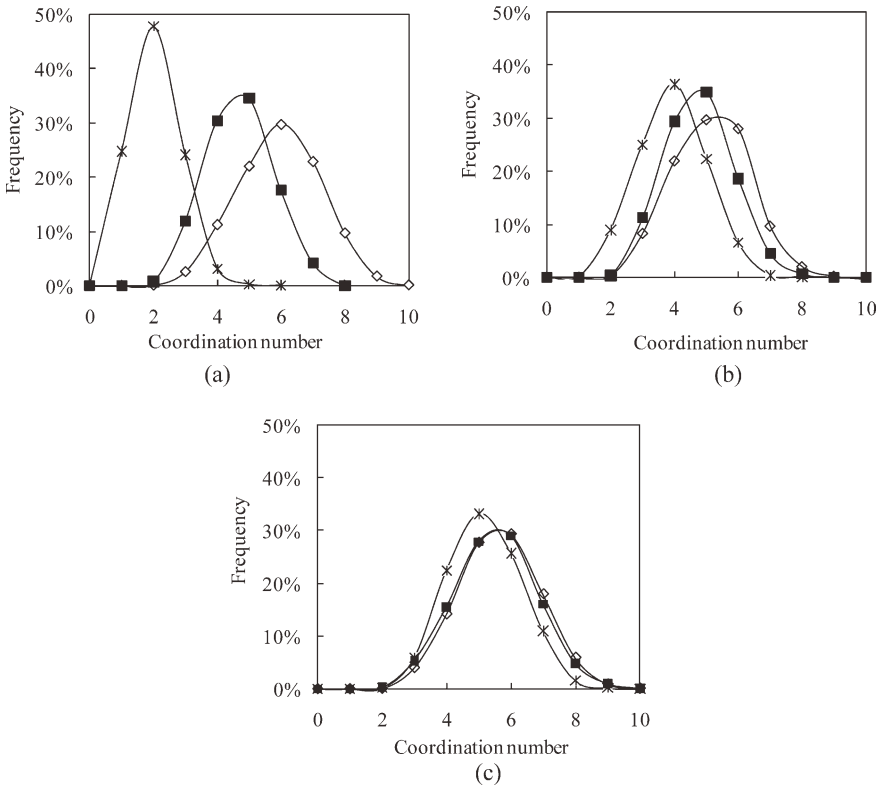

Figure 9. Variation of CN distributions with different: (a), particle size (✱, d = 5 μm; ■, d = 100 μm; and ◇, d = 1000 μm); (b), liquid density (✱, ρ_f = 2400 kg/m^3; ■, ρ_f = 2300 kg/m^3; and ◇, ρ_f = 1000 kg/m^3); and (c), liquid viscosity (✱, μ_f = 0.0001 kg/(ms); ■, μ_f = 0.01 kg/(ms); and ◇, μ_f = 0.1 kg/(ms)).

listed in Table 3. To eliminate the effect of gravity and size, we used a normalized force which is defined as the ratio of the forces and the mean value at the same height ($f = F_{i,h}/\langle F_h \rangle$). Unlike the packing of cohesionless particles, the force distributions show a well-defined peak around the mean value which becomes more prominent with decreasing particle size, and the curve moves to a more symmetrical form and becomes narrower. These distributions are consistent with those for fine particles packed in air or vacuum,[29] showing similar variations of the forces in the packing with the decreasing of packing fraction and suggesting the existence common relationships between packing fraction and the forces.

Our previous studies showed that packing fraction can be quantitatively linked to the averaged ratio of the van der Waals force to gravity, given by[13–15,30]:

$$\rho = \rho_0\left(1 - \exp\left(\alpha\chi^{\beta}\right)\right) \tag{4}$$

where ρ_0 is the packing fraction of cohesionless spheres, α and β are parameters relating to particle properties.[14] The force ratio χ_i for particle i can be given as:

$$\chi_i = \sum_j \left|\mathbf{F}_{ij}^{vdw}\right| / m_i \Delta g \tag{5}$$

where $\mathbf{F}_{ij}^{vdw}$ is the van der Waals force between particles i and j, and $\chi = \langle \chi_i \rangle$ is the averaged χ_i, and $\Delta g = (1 - \rho_f/\rho_p)g$ is the effective gravitational acceleration. The effective gravity force $m_i \Delta g$ under different conditions can be given as: (i), in vacuum, $m_i \Delta g = mg$[13]; (ii), settling in liquids, $m_i \Delta g = mg - |\mathbf{F}_{buoy}|$ [15]; and (iii), dead end filtration, $m_i \Delta g = mg - |\mathbf{F}_{buoy}| + |\mathbf{F}_{drag}|$.[16] This force ratio is similar to the so-called Bond number which has been used to describe the dynamic behavior of cohesive powders[31,32]. The differences are: (1) our treatment links the force ratio directly to the packing structure as the forces are summed over all the neighbour particles in a packing; and (2) the concept of effective gravity force is used to take into account of the buoyancy and drag forces.

Figure 17 plots ρ as a function of χ for all the cases studied in this work. For comparison, other results obtained from the simulation of the packing of fine particles in vacuum[13] and in filtration process[16] and the experimental studies of the random loosest packing formed in the fluidized bed[32] have also been included. Note that for the packing formed after defluidization, we have converted the Bond number ($|\mathbf{F}_{ij}^{vdw}|/mg$) for a single contact to our index $\chi_i (= \sum_j |\mathbf{F}_{ij}^{vdw}|/m_i \Delta g)$ by multiplying the mean CN estimated according to Eq. 3.

It can be seen that all the data can be described by Eq. 4, but α and β are different with different data sets. Specifically, at a given force ratio, packing fraction is the largest for the packing in vacuum, and the smallest for the packing from defluidization. The differences are attributed to the different packing conditions. For the packing in the air or vacuum, particles fall from a certain height and hit the packed bed with a relatively high velocity. Macroscopically, the

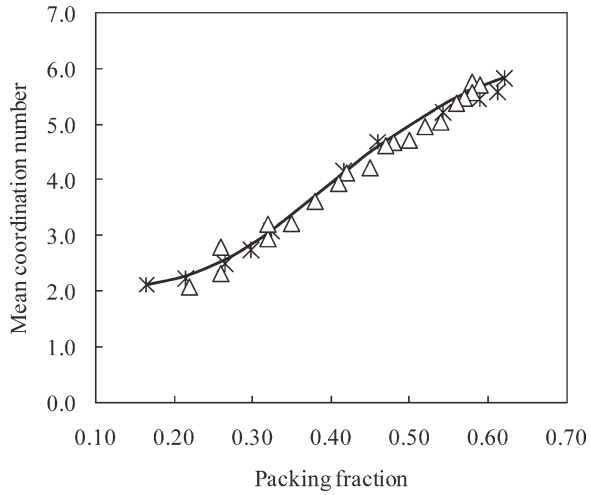

Figure 10. Averaged CN as a function of packing fraction for data obtained under different conditions. ⁎, the packing of fine particles[13]; Δ, the settling of particles in liquid[15]; and solid line is calculated from Eq. 3.

continuous impacts act like a compression force on the packing, which we name as the impact induced pressure (F^{IIP}). This force does not exist at the final stage but its resultant effect remains. On the other hand, such an impact is minimized by the upward air flow for the packing from defluidization, and is suppressed by liquid in a settling process. This impact induced pressure is an enhancement of the gravity and should be added in the effective gravity term in Eq. 5, giving a modified force ratio χ_i':

$$\chi_i' = \sum_j \left|\mathbf{F}_{ij}^{vdw}\right| / (m_i \Delta g + F_i^{IIP}) \tag{6}$$

Generally, F^{IIP} should be proportional to the impact force of a particle onto the packed bed. When particle i hits an existing bed, the average impact force F^{imp} can be calculated by its momentum loss divided by the collision time, i.e.,

$$F_i^{imp} = m_i V^{imp} / \Delta t^{imp} \tag{7}$$

where V^{imp} is the impact velocity, and Δt^{imp} is the collision time. The impact velocity can be estimated under different situations. In air or vacuum, the impact velocity depends on the drop height of a particle, with its average given by: $\overline{V}^{imp} = \sqrt{2g\overline{H}}$, where $\overline{H}$ is the average height of a particle to the underneath packed bed, which can be estimated from the initial and final packing fractions. For the packing formed from defluidization, particles are controlled to have a nearly zero impact velocity, i.e., $V^{imp} \approx 0$. For particles settling in a liquid or filtration, as the initial packing fraction is low and particles have enough height to reach their terminal velocity, the impact velocity can be estimated by the terminal velocity of a single settling particle, given by the Stoke's Law[33]: $V^{imp} = \frac{1}{18}\frac{(\rho_p - \rho_f)}{\mu_f} g d^2$ in settling, or $V^{imp} = \frac{1}{18}\frac{(\rho_p - \rho_f)}{\mu_f} g d^2 + U_f$ in filtration, where U_f is the liquid velocity. On the other hand, Δt^{imp} is not easy to estimate. Dimensional analysis shows that $\Delta t^{imp} \propto \sqrt{d/\Delta g}$. Thus Eq. 6 can be written as

$$\chi_i' = \sum_j \left|\mathbf{F}_{ij}^{vdw}\right| / (m_i \Delta g + \kappa \frac{m_i V^{imp}}{\sqrt{d/\Delta g}}) \tag{8}$$

where κ is a lumped parameter to be determined. In this work, we simply assume κ to be a constant. Replacing χ with χ' in Eq. 4, we obtain

$$\rho = \rho_0 \left(1 - \exp\left(\alpha \left\langle \sum_j \left|\mathbf{F}_{ij}^{vdw}\right| / \left(m_i \Delta g + \kappa m_i \frac{V^{imp}}{\sqrt{d/\Delta g}}\right)\right\rangle^{\beta}\right)\right) \tag{9}$$

Using all the data in Figure 17, the best fitting parameters in Eq. 9, obtained with the solver in Excel 2000, are $\alpha = -2.78$, $\beta = -0.195$ and $\kappa = 4.35$. The dependency of ρ on χ' is plotted in Figure 18. It can be seen that the data under different conditions can now collapse into a single curve, which verifies the generality of Eq. 9. It is also noticed that some data deviate

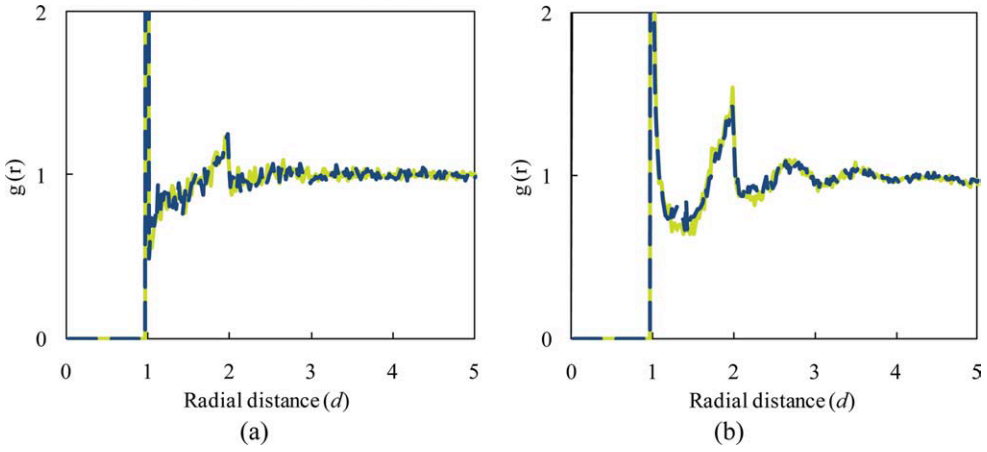

Figure 11. Comparisons of the RDF of different packings with similar packing fractions: (a), --, ρ = 0.546 (S1); and —, ρ = 0.549 (S2); and (b), --, ρ = 0.346 (S4); and —, ρ = 0.347 (S5).

[Color figure can be viewed in the online issue, which is available at wileyonlinelibrary.com].

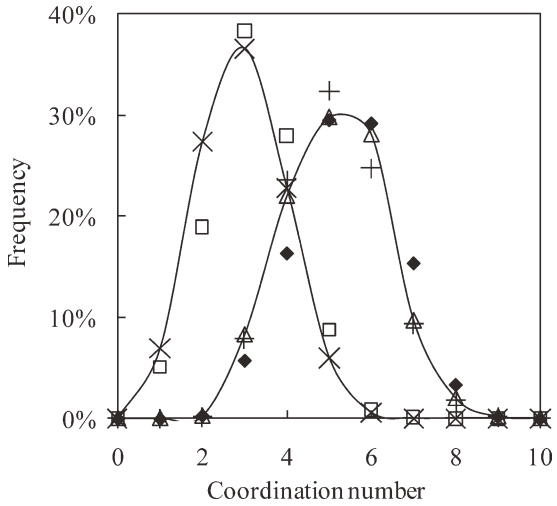

Figure 12. Comparisons of the CN distribution of different packings with similar packing fractions: (i) ◆, ρ = 0.546 (S1); +, ρ = 0.549 (S2); and Δ, ρ = 0.547 (S3); and (ii), □, ρ = 0.346 (S4); and ×, ρ = 0.347 (S5).

from the curve. This is probably due to the simplified treatment of F^{IIP} in the current work. Moreover, it is known that in addition to particle density, other particle properties such as friction and restitution coefficients will affect packing, e.g., ρ_0 in Eqs. 4 or 9,[34–36] it is not clear how they may affect the settling of particles in liquids. Further studies are, therefore, necessary to overcome these problems. Nonetheless, as demonstrated below, Eq. 9 is very useful to assess the effects of liquid-related properties.

Effects of liquid properties on the ρ-d relationship

Equation 9 quantifies the effects of key variables on the packing fraction. It allows a wide range of packings formed under different conditions to be discussed analytically. Here, it is applied to study the effects of liquid properties on the

Table 3. List of Selected Simulated Cases

Case	d (μm)	ρ_f (kg/m^3)	μ_f (kg/(ms))	A ($\times$ 10^{-20}J)	ρ
S1	100	1000	0.001	0.57	0.546
S2	1000	2400	0.001	6.5	0.549
S3	250	1000	0.001	6.5	0.547
S4	50	2200	0.01	6.5	0.346
S5	20	1000	0.001	6.5	0.347

ρ-d relationship which represents an important aspect in the study of particle packing.[30] Similar to the above simulation studies, when studying the effect of a variable, other variables are set to their base values unless otherwise stated. Moreover, for simplicity it is assumed that the van der Waals force for particle i can be estimated as[20]: $|\mathbf{F}_{ij}^{vdw}| = \frac{A}{12}\frac{d}{h_{\min}^2}$. In this case, χ_i' can be written as a function of A, d, ρ_f, and μ_f:

$$\chi_i' \approx \frac{A}{2h_{\min}^2 g d^2(\rho_p - \rho_f)} \cdot \frac{1}{1 + (\kappa\sqrt{\rho_p}/18)\sqrt{d^3}\sqrt{(\rho_p - \rho_f)/\mu_f^2}} \tag{10}$$

The relationship between packing fraction and particle size has been well established for the packing of particles in air: ρ decreases with d when d is smaller than 100 μm. This is because that the gravity decreases faster than the van der Waals force with the decrease of d, which increases the difficulties for particle re-arrangements.[13,37] For particle settling in liquids, the ρ-d relationship is dependent on liquid properties. Figure 19 shows the relationships between ρ and d with different Hamaker constants, liquid densities or liquid viscosities. Generally, ρ increases from almost zero to a maximum value (ρ_0) with the increase of d, which is similar to that in air. ρ_0 is the packing fraction for noncohesive particles. However, quantitatively, the ρ-d relationship is different under different conditions. Figure 19a shows that with a smaller A, ρ increases faster with the increase of d and reaches ρ_0 at a smaller d. This is because a lower A results in a lower van der Waals force under the same d. When $A = 0$, the packing fraction will always be ρ_0 and the change of d has no effect on

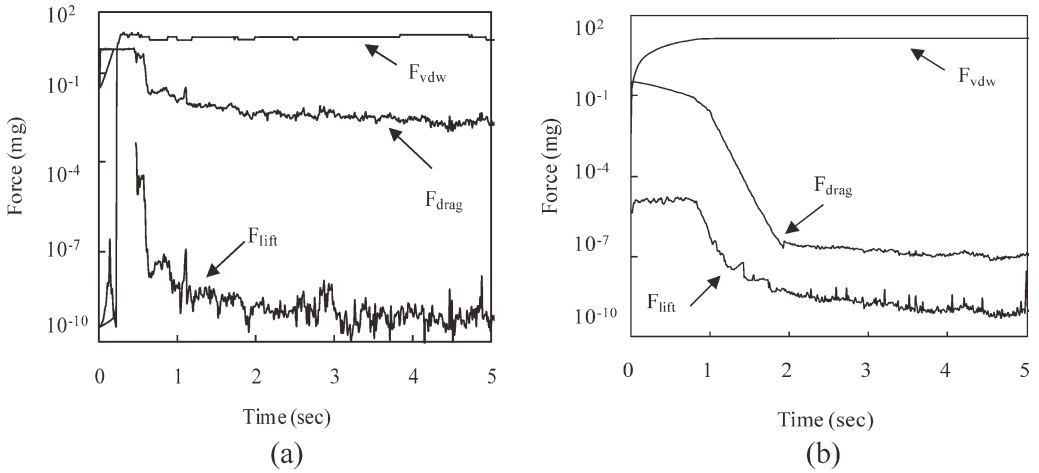

Figure 13. Variation of: (a), the forces of a single particle with time; and (b), the average forces of all particles with time during the packing process.

All parameters are at their base values.

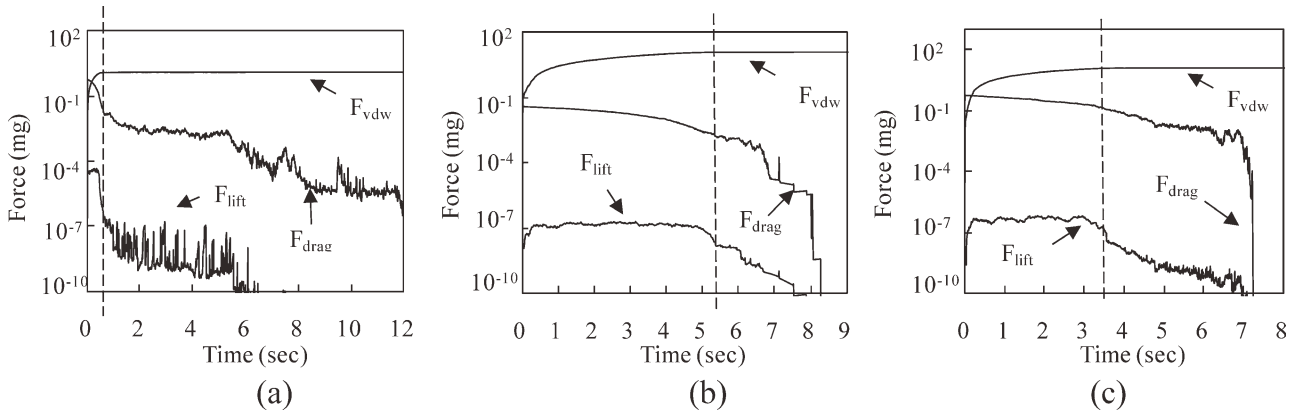

Figure 14. Variation of the average forces on particles with time during a settling process under different conditions: (a), $A = 5.7 \times 10^{-21}$ J (lower Hamaker constant than Figure 13(b)); (b), $\rho_f = 2200$ kg/m^3 (higher liquid density); and (c), $\mu_f = 0.01$ kg/(ms) (higher liquid viscosity).

The vertical dashed line roughly separates the free settling and rearranging periods.

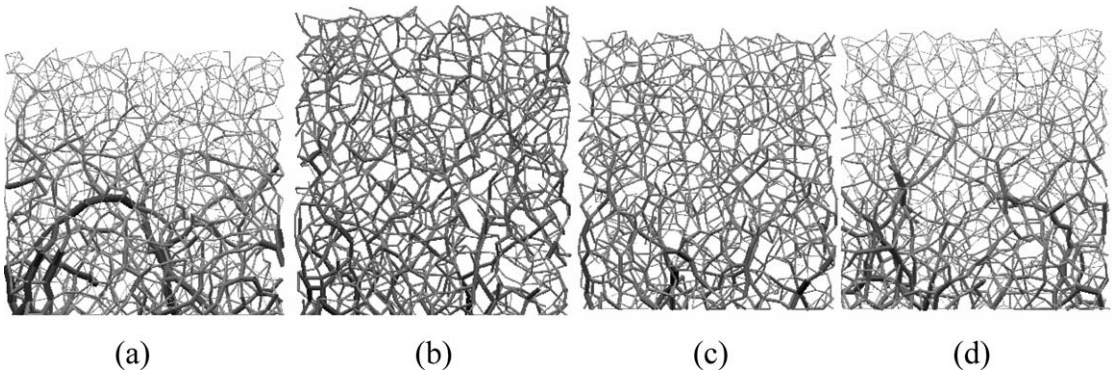

Figure 15. Contact force network in a cross section of thickness of 2 particle diameters: (a), base case; (b), $d = 50$ μm (smaller size); (c), $\rho_f = 2400$ kg/m^3 (higher liquid density); and (d), $\mu_f = 0.1$ kg/(ms) (higher liquid viscosity).

Darker and thicker branches represent larger contact forces.

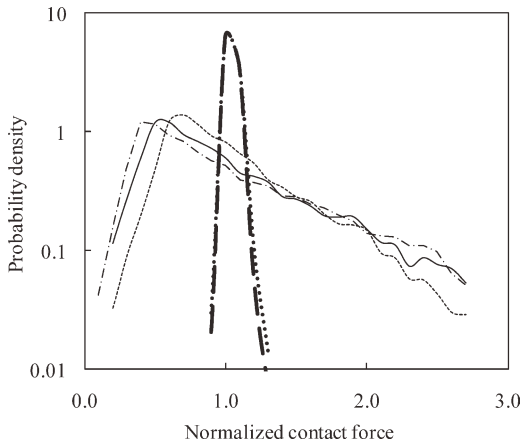

Figure 16. Statistical distributions of the normalized contact forces for the packings listed in Table 3. –.–, $\rho = 0.546$ (S1); ---, $\rho = 0.549$ (S2); —, $\rho = 0.547$ (S3); — —, $\rho = 0.346$ (S4); ------, $\rho = 0.347$ (S5).

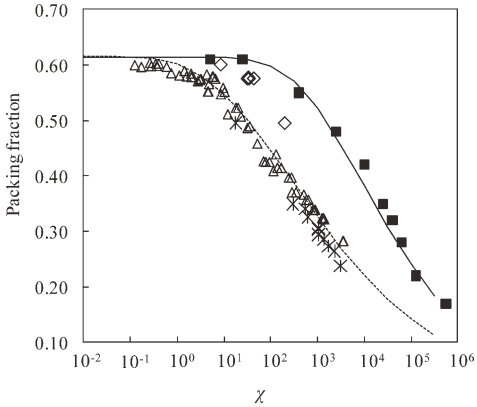

Figure 17. Packing fraction as a function of the force ratio χ. Points are data from simulations of: ■, packing of fine particles[13]; Δ, settling of particles in liquid[15]; ◇, packing formed in filtration[16]; and ✳, packing formed from defluidization.[32]

Lines are the results calculated according to Eq. 4: solid line,[13] $\rho_0 = 0.616$, $\alpha = -7.750$ and $\beta = -0.256$; dotted line,[15] $\rho_0 = 0.616$, $\alpha = -2.457$, and $\beta = -0.212$.

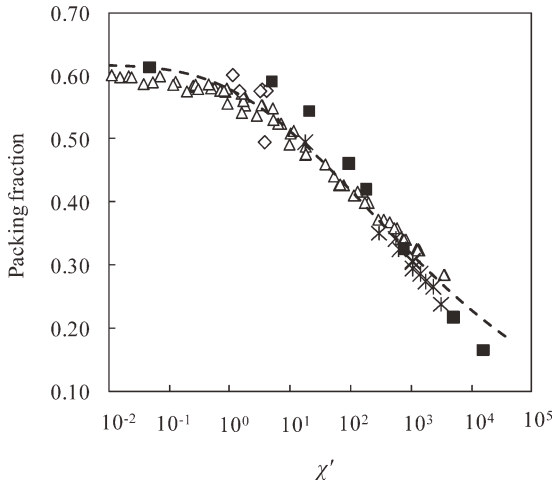

Figure 18. Packing fraction as a function of the force ratio χ' from different data sets: ■, packing of fine particles; Δ, settling of particles in liquid; ◇, packing formed in filtration; and ✳, packing formed from defluidization.

Lines are results calculated from Eq. 4: $\rho_0 = 0.616$, $\alpha = -2.78$, $\beta = -0.195$.

ρ, which highlights the key role of the cohesion force in forming the loose packing, and is in agreement with the previous discussions.[30] Figures 19b, c show that for liquids with higher density and/or higher viscosity, ρ rises slower with the increase of d and approaches ρ_0 at a larger d, as Eq. 10 shows the increase of ρ_f or μ_f will decrease χ_i' and hence ρ.

It was thought that packing fraction decreases with the effective gravity ($m\Delta g$).[17] However, as pointed out in our previous study,[15] packing fraction should be related to not only the effective gravity but also the cohesive force. It is the ratio between the cohesive force to the effective gravity that controls the final packing. Figure 20 demonstrates that ρ decreases with the effective gravitational acceleration, which is related to the liquid density, when the impact velocity is assumed to be zero. It can be seen that for different sized particles, the ρ-$m\Delta g$ relationship varies with particle size because of the varied cohesive force. At a given effective gravitational acceleration, ρ is still smaller for a smaller d. This is because the effective gravity is controlled by particle mass which is proportional to d^3, and increases faster than the van der Waals force which is proportional to d.

One interesting question is what will be the relationship between ρ and d if the effective gravity is constant? By varying the liquid density for different particle sizes, such condition can be obtained. Figure 21 shows the results obtained under different effective gravity forces, calculated according to Eqs. 4 and 10. Note that in this figure, A is set to be 1.0×10^{-21} J to give the most comparable simulation results to the experimental data. It is clear that under the same effective gravity, ρ decreases with increasing d. The experimental data, although limited, indeed confirms the

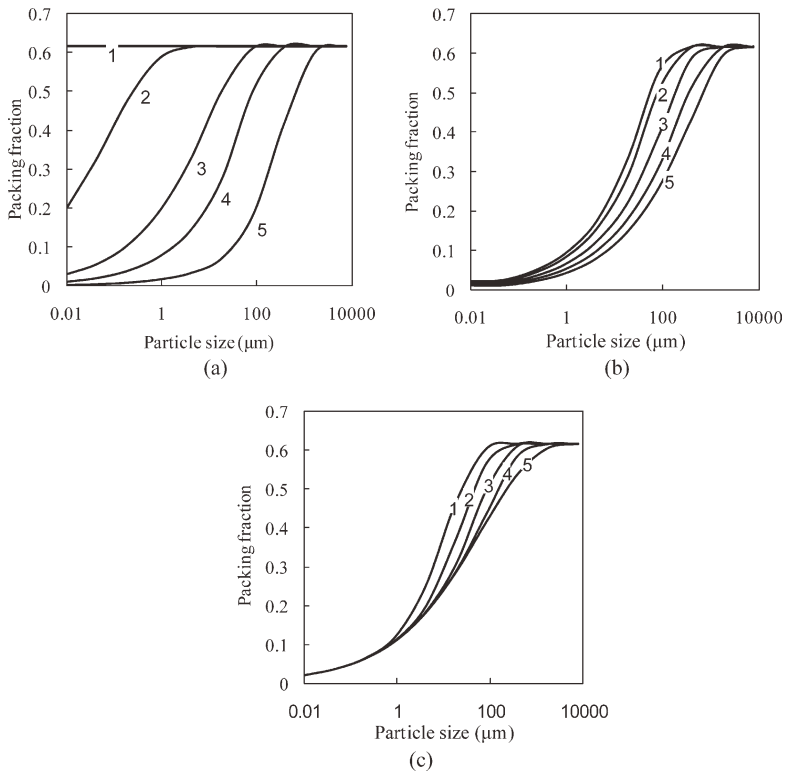

Figure 19. Packing fraction as a function of particle size for different: (a), Hamaker constants (line 1, $A = 0$ J; line 2, $A = 1.0 \times 10^{-25}$ J; line 3, $A = 1.0 \times 10^{-22}$ J; line 4, $A = 1.0 \times 10^{-19}$ J; and line 5, $A = 1.0 \times 10^{-16}$ J); (b), liquid densities (line 1, $\rho_f = 0$ kg/m^3; line 2, $\rho_f = 1000$ kg/m^3; line 3, $\rho_f = 2000$ kg/m^3; line 4, $\rho_f = 2300$ kg/m^3; and line 5, $\rho_f = 2400$ kg/m^3); and (c), liquid viscosities (line 1, $\mu_f = 1.0 \times 10^{-5}$ kg/(ms); line 2, $\mu_f = 1.0 \times 10^{-4}$ kg/(ms); line 3, $\mu_f = 1.0 \times 10^{-3}$ kg/(ms); line 4, $\mu_f = 1.0 \times 10^{-2}$ kg/(ms); and line 5, $\mu_f = 1.0$ kg/(ms)).

analytical results. Obviously, the decrease of ρ with the increasing d is opposite to that shown in Figures 5b and 19. However, they are actually consistent with each other because they are all described by Eq. 9. Figures 5b and 19 show that ρ-d relationships when $m\Delta g$ varies relating to different variables, while Figure 21 shows the ρ-d relationships when $m\Delta g$ is constant. Constant $m\Delta g$ is difficult to realise in physical experiments. In fact, the ρ-d relationships reported in the literature were all obtained under the condition that $m\Delta g$ is proportional to d^3. However when $m\Delta g$ is constant, increasing d will increase the van der Waals force and hence decrease χ', resulting in decreased ρ. Obtained for different constant $m\Delta g$, the results in Figure 21 are therefore very illustrative in highlighting the importance of cohesive forces.

Conclusions

The effects of material properties on the packing formed by settling uniform spheres in liquids were studied by DEM model. The results show that packing fraction decreases with the decreasing particle size or increasing Hamaker constant, liquid density and viscosity. With decreasing packing fraction, the packing structure changes in a similar way. In general, the subpeaks of the RDF diminish gradually, showing a decrease of the local order. The average CN decreases and its distribution becomes narrower. The packings formed under different conditions with the same packing fraction are found to have almost the same RDF and CN distributions, demonstrating that they have the close packing structures. Therefore, the structures of cakes can be described by a single macroscopic parameter, i.e., packing fraction or porosity.

The effects of variables related to material properties on packing are through their effects on the process-related and process-independent forces during the settling process. The increase of the Hamaker constant, liquid density or viscosity increases the cohesion and liquid-particle forces, producing an increased resistant force to particle flow and re-arrangement and hence a decreased packing fraction.

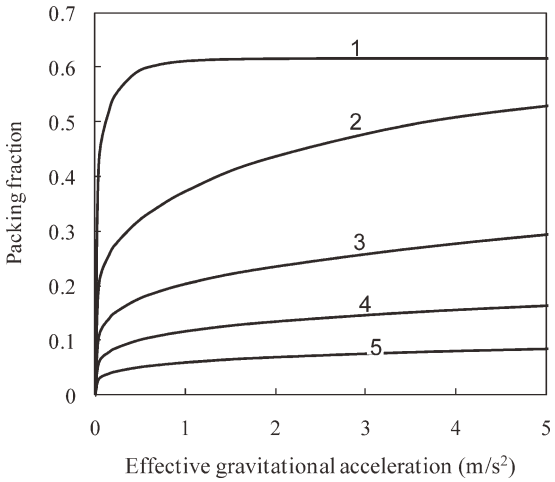

Figure 20. Packing fraction as a function of effective gravitational acceleration (or liquid density) for different particle sizes: line 1, d = 1000 μm; line 2, d = 100 μm; line 3, d = 20 μm; line 4, d = 5 μm; and line 5, d = 1 μm, here V^{imp} = 0.

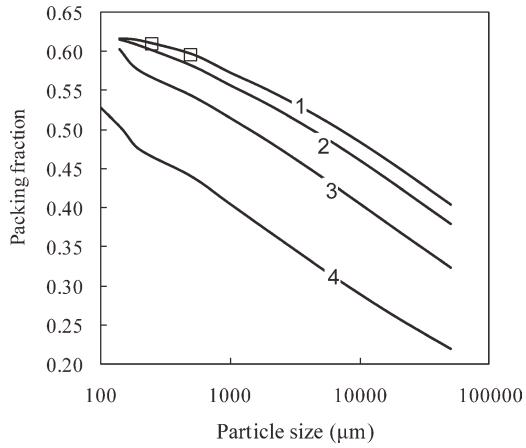

Figure 21. Packing fraction as a function of particle size under different effective gravities.

Lines are calculated by Eqs. 4 and 10, using $A = 1.0 \times 10^{-21}$ J: line 1, $m\Delta g = 5.68 \times 10^{-8}$ kg/ms^2; line 2, $m\Delta g = 4.42 \times 10^{-8}$ kg/ms^2; line 3, $m\Delta g = 3.16 \times 10^{-8}$ kg/ms^2; and line 4, $m\Delta g = 2.59 \times 10^{-8}$ kg/ms^2; □ is the experimental data.

A general equation has been formulated to describe the dependence of packing fraction on inter-particle forces such as the gravity, the cohesive force, the effective buoyancy force, and the impact induced pressure force. This equation can generally be used to investigate the effects of particle and liquid properties under different conditions, at least as the first approximation. It also shows the relationship between packing fraction and particle size is very much condition-dependent and hence complicated.

Acknowledgment

The authors are grateful to the Australian Research Council for the financial support of this work.

Literature Cited

1. Dickenson TC. *Filter and Filtration Handbook*. New York: Elsevier Science Ltd, 1997.
2. Tien C. Cake filtration research—a personal view. *Powder Technol*. 2002;127:1–8.
3. Burger R, Concha F, Karlsen KH. Phenomenological model of filtration processes: 1. Cake formation and expression. *Chem Eng Sci*. 2001;56:4537–4553.
4. Olivier J, Vaxelaire M. Modelling of cake filtration: an overview. *Separ Sci Technol*. 2007;42:1667–1700.
5. Tassopoulos M, O'Brien JA, Rosner DE. Simulation of microstructure/mechanism relationships in particle deposition. *AIChE J*. 1989; 35:967–980.
6. Houi D, Lenormand R. Experimental and theoretical study of particle accumulation at the surface of a filter. Proceedings of the 4th World Filtration Congress, Ostend, Belgium, 1986.
7. Lu WM, Hwang KJ, Ju SC. Studies on the mechanism of cross-flow filtration. *Chem Eng Sci*. 1993;48:863–872.
8. Hwang KJ, Liu HC, Lu WM. Local properties of cake in cross-flow microfiltration of submicron particles. *J Membrane Sci*. 1998;138: 181–192.
9. Fu LF, Dempsey BA. Modeling the effect of particle size and charge on the structure of the filter cake in ultrafiltration. *J Membrane Sci*. 1998;149:221–240.

10. Schwarzer S. Sedimentation and flow through porous media: simulating dynamically coupled discrete and continuum phases. *Phys Rev E*. 1995;52:6461.
11. Cundall PA, Strack ODL. A discrete numerical model for granular assemblies. *Géotechnique*. 1979;29:47.
12. Yu AB. Discrete element method—an effective method for particle scale research of particulate matter. *Eng Comput*. 2004;21:205.
13. Yang RY, Zou RP, Yu AB. Computer simulation of the packing of fine particles. *Phys Rev E*. 2000;62:3900–3908.
14. Yang RY, Zou RP, Yu AB. Effect of material properties on the packing of fine particles. *J Appl Phys*. 2003;94:3025–3034.
15. Dong KJ, Yang RY, Zou RP, Yu AB. Role of interparticle forces in the formation of random loose packing. *Phys Rev Lett*. 2006;96: 145505.
16. Dong KJ, Zou RP, Yang RY, Yu AB, Roach G, DEM simulation of cake formation in sedimentation and filtration. *Miner Eng*. 2009;22: 921–930.
17. Onoda GY, Liniger EG. Random loose packings of uniform spheres and the dilatancy onset. *Phys Rev Lett*. 1990;64:2727–2730.
18. Brilliantov NV, Spahn F, Hertzsch J, Pöschel T. Model for collisions in granular gases. *Phys Rev E*. 1996;53:5382–5392.
19. Langston PA, Tüzün U, Heyes DM. Discrete element simulation of granular flow in 2d and 3d hoppers: dependence of discharge rate and wall stress on particle interactions. *Chem Eng Sci*. 1995;50:967.
20. Israelachvili JN. *Intermolecular and Surface Forces*, 2nd ed. Academic: London, 1991.
21. Xu BH, Yu AB. Numerical simulation of the gas-solid flow in a fluidized bed by combining discrete particle method with computational fluid dynamics. *Chem Eng Sci*. 1997;52:2785–2809.
22. Crowe C, Sommerfeld M, Tsuji Y. *Multiphase Flows with Droplets and Particles*. CRC Press, Boca Raton, LISA, 1998.
23. Derjaguin BV, Muller VM, Toporov YP. Effect of contact deformations on the adhesion of particles. *J Colloid Interf Sci*. 1975;53:314–326.
24. Johnson KL, Kendall K, Roberts AD. Surface energy and the contact of elastic solids. *Proc R Soc (Lond) A*. 1971;324:301.
25. Muller VM, Yushchenko VS, Derjaguin BV. On the influence of molecular forces on the deformation of an elastic sphere and its sticking to a rigid plane. *J Colloid Interf Sci*. 1980;77:91–101.
26. Tykhoniuk R, Tomasa J, Luding S, Kappl M, Heim L, Butt H. Ultrafine cohesive powders: from interparticle contacts to continuum behaviour. *Chem Eng Sci*. 2007;62:2843–2864.
27. Zou RP, Yu AB. Wall effect on the packing of cylindrical particles. *Chem Eng Sci*. 1996;51:1177.
28. Yang RY, Zou RP, Yu AB, Choi SK. Characterization of interparticle forces in the packing of cohesive fine particles. *Phys Rev E*. 2008;78:031302.
29. Cates ME, Wittmer JP, Bouchaud J, Claudin P. Jamming, force chains, and fragile matter. *Phys Rev Lett*. 1998;81:1841–1844.
30. Yu AB, Feng CL, Zou RP, Yang RY. On the relationship between porosity and interparticle forces. *Powder Technol*. 2003; 130:70–76.
31. Valverde JM, Quintanilla MAS, Castellanos A, Lepek D, Quevedo J, Dave RN, Pfeffer R. Fluidization of fine and ultrafine particles using nitrogen and neon as fluidizing gases. *AIChE J*. 2008;54:86–103.
32. Valverde JM, Castellanos A. Random loose packing of cohesive granular materials. *Europhys Lett*. 2006;75:985–991.
33. Batchelor G.K. *An Introduction to Fluid Dynamics*. Cambridge University Press, New York, 1967.
34. Gray WA. *The Packing of Solid Particles*. London: Chapman and Hall, 1969.
35. German RM, *Particle Packing Characteristics*. Princeton, New Jersey: Metal Powder Industries Federations, 1989.
36. Zhang ZP, Liu LF, Yuan YD, Yu AB. A simulation study of the effects of dynamic variables on the packing of spheres. *Powder Technol*. 2001;116:23–32.
37. Mizuno M, Fukaya A, Jimbo G. The estimation of packing characteristics by centrifugal compaction of ultrafine particles. *KONA*. 1991;9:19.

Manuscript received Dec. 9, 2010, and revision received Apr. 26, 2011.